Article

Spot Weld Inspections Using Active Thermography

Simon Verspeek [1,*], Bart Ribbens [1], Xavier Maldague [2] and Gunther Steenackers [1]

1. Research Group InViLab, Department Electromechanics, Faculty of Applied Engineering, University of Antwerp, Groenenborgerlaan 171, 2020 Antwerp, Belgium; bart.ribbens@uantwerpen.be (B.R.); gunther.steenackers@uantwerpen.be (G.S.)
2. Computer Vision and Systems Laboratory, Department of Electrical and Computer Engineering, Université Laval, Quebec, QC G1V 0A6, Canada; xavier.maldague@gel.ulaval.ca
* Correspondence: simon.verspeek@uantwerpen.be; Tel.:+32-3-265-87-94

Abstract: Spot welds have a significant part in the creation of automotive vehicles. Since the integrity of, for example, a car, is dependent on the performance of multiple welds, it is important to ensure the quality of each spot weld. Several attempts have been made in order to determine the quality of spot welds, but most of them do not focus on the applicability in the manufacturing process. Spot weld inspections are often performed using back heating. However, during manufacturing, robotic inspections are desired, and since the bodywork of a car is a complex shape, the accessibility from the inside of the vehicle is minor. Therefore, inspections using front heating are more suitable. In this manuscript, multiple excitation methods are compared as well as different post-processing techniques. The used excitation techniques can be divided into light heating and inductive heating. Light heating is further divided in lock-in thermography and pulse thermography. The used post-processing techniques are principle component analysis and fast Fourier transform. Inductive heating turns out to be the most suitable measurement technique since it is fast and can be performed as front and back heating. Both investigated post-processing techniques deliver suitable information, such as relief images and information of the internal structure of the spot weld.

Keywords: active thermography; non-destructive inspection; spot welds

1. Introduction

Performing quality inspections during manufacturing has increased enormously in the last decades, and more and more manufacturers are discovering the use of non-destructive inspection methods. Using non-destructive testing, it is no longer needed to manufacture additional parts in order to submit them to destructive inspections. Those inspections are performed in a variety of fields, such as aircraft construction, metal structure manufacturing, composite manufacturing, etc. Several different techniques are being used in order to examine the structural integrity of the manufactured parts. Amosov et al. [1] performed ultrasonic testing on riveted joints in aviation construction, Deepak et al. [2] compared different non-destructive inspection techniques to assess the quality of welded joints and Jasiūnienė et al. [3] performed ultrasonic testing on complex titanium and carbon fiber composite joints. It is proven that non-destructive testing can offer a reliable inspection method in order to investigate the structural integrity of materials and joints. In the automotive industry, many spot welds are used to combine parts together. On average, the body work of a car alone consists already of 5000 spot welds [4]. Nowadays, the quality of the spot weld is investigated using destructive research, resulting in many disadvantages. If the quality of the spot weld is not sufficient, a larger batch of spot welds will be disapproved since not every single spot weld can be tested. Therefore, car manufacturers search for alternative solutions in non-destructive inspections. An easy inspection method can be found in visual inspections; however, these examinations can only be performed by someone skilled in the art. An alternative can be found in penetrant testing. This technique is suitable to detect

cracks, but is not capable of showing defects inside the material. Besides penetrant testing, another surface examination technique can be found in eddy current testing [5–7]. Performing subsurface inspections is possible using ultrasonic testing, but extreme accuracy is needed to place the transducer in the middle of the spot weld. Performing visual surface inspection of spot welds is not sufficient since a spot weld can look decent although no internal structure change has occurred. As explained in [8], a proper spot weld contains multiple sections. The weld nugget has a different internal structure in comparison to the region around it. Therefore, it is important to inspect the surface of a spot weld as well as the internal structure. An alternative approach can be found in active thermography for non-destructive inspections [8–10]. Several efforts have been made regarding the use of active thermography for spot weld inspections [11–14]. Scientific research often focuses on the ability to inspect spot welds using a specific measurement setup. A. Runnelmalm and A. Appelgren [5] and Jonietz et al. [14] performed thermography using light sources as external heating, and Kastner et al. [12] and Schlichting et al. [13] combined thermography with laser excitation. However, in a manufacturing process, not every measurement technique can be used. It is, for instance, possible to inspect spot welds using laser thermography, but due to safety issues, it is not suitable to be used in the production hall without extensive safety precautions. This manuscript focuses on finding the most optimal measurement setup to perform active thermography inspections during the manufacturing process. Multiple excitation methods are described in this manuscript, divided in several paragraphs based on the used heating method. For each measurement setup, a variety of parameters is tested and compared. Besides a variation in excitation parameters, a comparison between two post-processing techniques is performed for each excitation type. The used measurement setups can be found in Section 2, Materials and Methods. Section 3 describes the influence of the different parameter sets and post-processing techniques.

2. Materials and Methods

Nine different samples are inspected using different active thermography techniques in order to find the best inspection method. The samples are divided into two groups: A and B. The A-series comprises four samples with the same thickness (2.5 mm) and one sample that is 3.15 mm thick. All samples of series B have a thickness of 2.5 mm. An RGB image of the samples can be seen in Figure 1. The A-series samples are used to find the best measurement setup for the inspection of spot welds using active thermography. The B-series will function as a validation set to test the best suitable measurement method.

The parameters used to weld the samples can be found in Table 1.

Table 1. Parameters used to generate the samples.

Sample	1A	2A	3A	4A	5A	1B	2B	3B	4B
Current [kA]	8	6	3.5	5	16	8	6	3.5	5
Weldtime [ms]	400	200	600	200	300	400	200	600	200
Force [kN]	3	2.6	3	3.5	2.8	3	2.6	3	3.5

The camera used for these experiments is a FLIR X6540sc with a 25 mm lens. This cooled camera has a spectral range between 1.5 and 5.5 μm and a thermal sensitivity smaller than 25 mK. The thermal camera is mounted on a tripod and placed in front of the sample.

2.1. Excitation Methods

Different excitation techniques are used in order to find the optimal measurement setup for spot-weld inspections. The used techniques can be divided by the heating mechanics used: light heating and inductive heating. Heating the samples using halogen lamps is performed using lock-in thermography and pulse thermography.

2.1.1. Light Heating

Two halogen lamps of 2 kW each are used as a heating source. These lamps are from the brand Edevis and can be found online as the OTvis system. The lamps are mounted on a tripod and placed on either side of the thermal camera. The measurement setup for the light heating experiments can be found in Figure 2 , and the according parameter values are discussed in Table 2.
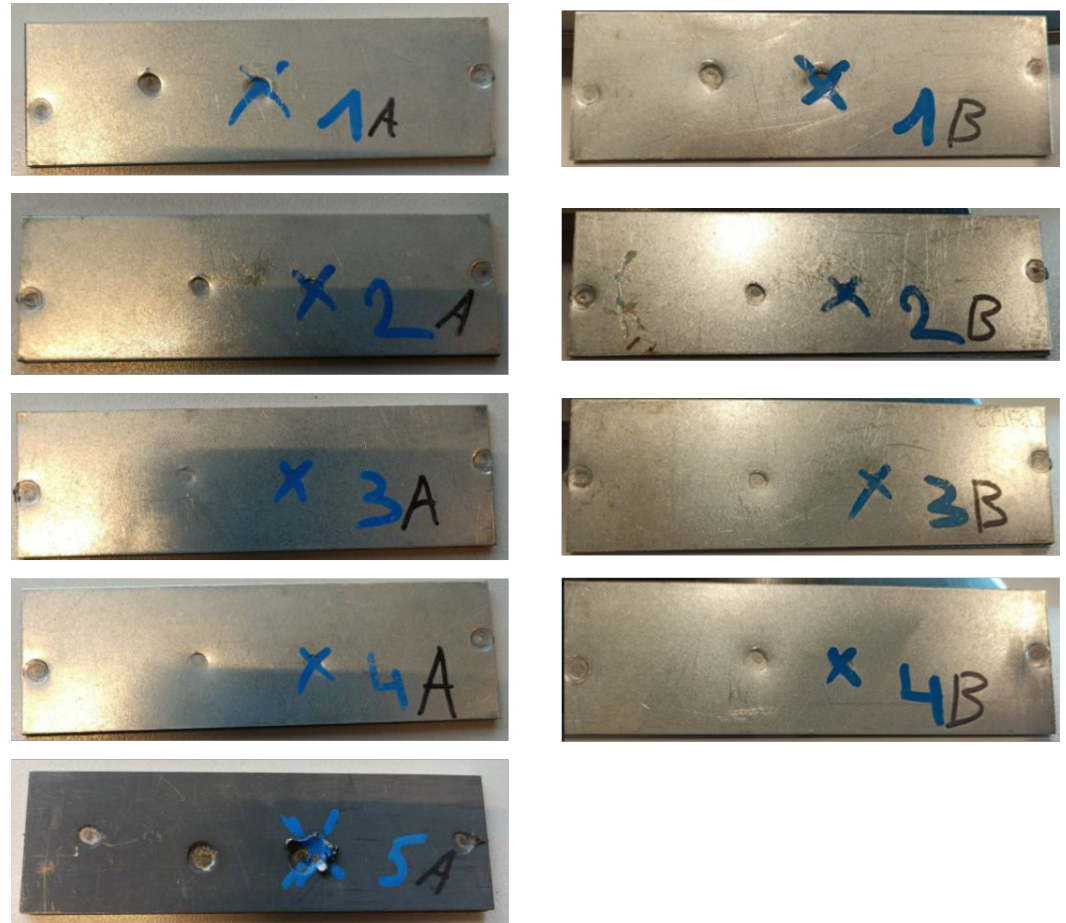
Figure 1. Nine samples, divided into two series. The A-series consists of four samples with a thickness of 2.5 mm (1–4) and sample 5A is 3.15 mm thick. The B-series only consists of four samples with a thickness of 2.5 mm. The spot weld highlighted by the blue cross is the inspected spot weld for each sample.

Table 2. Parameters used during light heating measurements. A representation of the parameters can be found in Figure 2.

Parameter	Value
Distance camera—sample 'L1' [m]	0.44
Distance lamp—lamp 'L2' [m]	0.88
Distance lamp—sample 'L3' [m]	0.44
Angle lamp—camera [°]	45
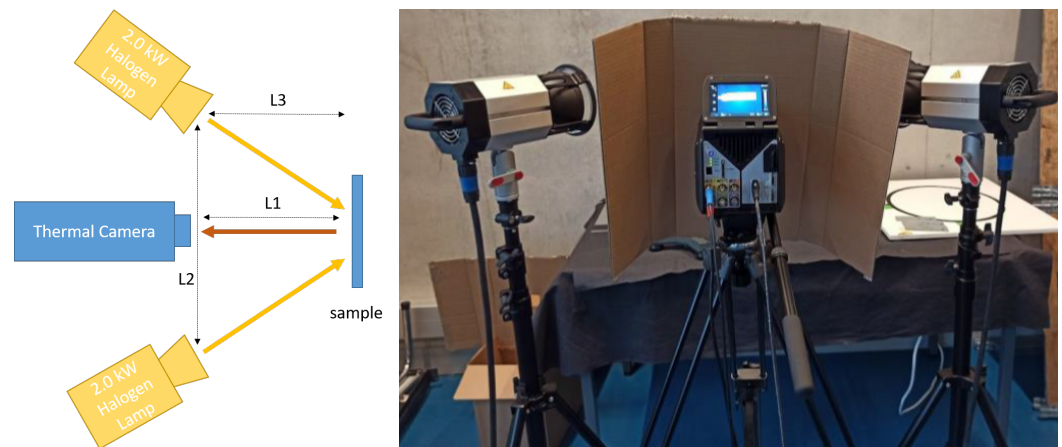
Figure 2. Visualization of the measurement setup used for light heating experiments. The **left** image is a schematic representation of the setup, and the **right** image is taken during measurements. The cardboard is placed in front of the thermal camera to prevent the radiation emitted by the camera reflecting on the sample to be inspected.

2.1.2. Induction Heating

The measurements performed in this manuscript using induction heating are performed using a 1.5 kVA Leon LIH-15 heater. The heating energy is transferred to the sample through an induction coil containing two windings. The induction heating device is mounted using a clamp at the desired location and distance next to the sample to be inspected. The sample is heated using inductive step heating. The pulse duration can be found in Table 3. A visualization of the measurement setup can be seen in Figure 3.
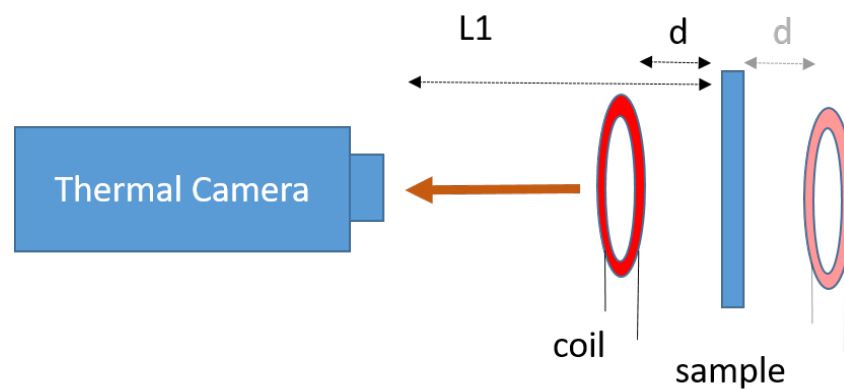
Figure 3. Schematic overview of the measurement setup used for induction thermography measurements. Both front and back heating are performed. The parameter values can be found in Table 4.

Table 3. Parameters used during inductive thermography of spot welds. Each sample of the A-series is inspected using these parameters.

	Parameter Set 1	Parameter Set 2	Parameter Set 3
Induction time front heating [s]	5	10	19
Induction time back heating [s]	4	8	15

Table 4. Parameter values used during induction heating measurements for the inspection of spot welds. A visual representation of the parameters can be found in Figure 3.

Parameter	Front Induction Heating	Back Induction Heating
Distance camera—sample 'L1' [m]	0.053	0.55
Distance sample—coil 'd' [m]	0.03	0.025

3. Results

Due to welding, the metallic parts are connected together, resulting in a place where the heat can be distributed through more material. In addition the internal structure of the metal is changed in welds that are properly performed. Using infrared thermography, a difference in heat transfer can be observed between the welded area and the rest of the sample. The welded regions will show different cooling down in comparison to the non welded regions. This difference can be emphasized using post-processing. The difference in internal structure of a decent weld will also result in a difference in cooling down and can again be emphasized using post-processing. A more thorough explanation on why thermography can be used to inspect spot welds can be found in [14].

The results of the different heating techniques and post-processing are shown and discussed below. The results are divided into different sections depending on the used excitation method.

3.1. Lock-in Thermography Using Light Heating

Since lock-in thermography is based on sinusoidal excitation, the optimal amplitude and frequency combination has to be found in order to increase the contrast of the interesting regions. The amplitude corresponds to the amount of energy injected in the sample to be inspected; the frequency on the other hand determines the time within which the heating energy is injected into the sample. A lower frequency results in a longer heating time. Multiple experiments were performed on one sample in order to find suitable parameter combinations. These experiments have shown that a lower frequency (e.g., 0.05 Hz) results in better images. Higher frequencies (e.g., 1.4 Hz) generated noisy thermograms. The influence of the amplitude was determined as well, and a minimal amplitude of 60% of the maximum power was needed to be able to perform analyses on the thermal data. For each sample, two parameter combinations were used. The used parameter sets can be found in Table 5.

Table 5. Parameter combinations used for the inspection of each sample using lock-in thermography. The number of periods is kept constant at a value of two, and the amplitude is kept constant at 80% of the maximum power.

	Parameter Set 1	Parameter Set 2
Frequency [Hz]	0.05	0.4
Amplitude	80%	80%
Number of periods	2	2

The experiments are analyzed using both fast Fourier transform (FFT) and principle component analysis (PCA). PCA is based on singular value decomposition, and the goal of this technique is to reduce the amount of variables while losing the least amount of relevant information. FFT, on the other hand, is based on the approximation of the data through the sum of harmonic waves. The phase and amplitude can be calculated from this approximation. A thorough explanation on both post-processing techniques can be found in [15,16]. Investigating the FFT images in Figure 4, it is visible that samples 1A, 2A and 3A show a closed circular shape around the spot weld and 4A only shows a part of the circle. The images of sample 5A do not suffice for making a conclusion about the shape of the spot weld. Another interesting aspect of a spot weld is the internal material structure

inside the spot weld. Spot welds should have a different internal structure in comparison to the material around it. In samples 1A, 2A and 5A, a different thermal behaviour can be detected inside and outside the spot weld, which a different material structure might suggest. In samples 3A and 4A, this phase shift is not visible. Besides the Fourier analysis, PCA is performed in order to generate relief images. In the PCA images of samples 1A and 2A, the circular shape of the spot weld is visible. Sample 2A has the most clear circle shape. Sample 3A is less visible in the PCA in comparison to the FFT analysis, but the circle around the spot weld is still visible. Sample 4A has no closed boundary, and sample 5A shows a capricious relief. The images can be seen in Figure 5.
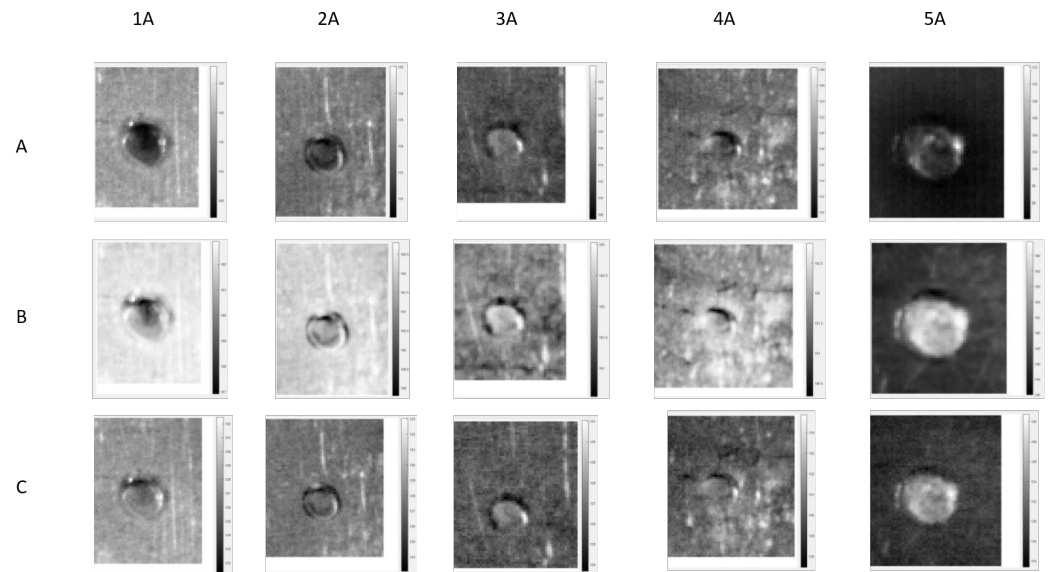
Figure 4. Snapshots taken from fast Fourier analysis for the different samples during three measurements. Experiment (**A**) is performed using an excitation frequency of 0.05 Hz and a Fourier frequency of 0.025 Hz, experiment (**B**) uses an excitation frequency of 0.05 Hz and a Fourier frequency of 0.05 Hz, and during experiment (**C**), the samples are excited using a frequency of 0.4 Hz and analyzed using a Fourier frequency of 0.2 Hz. Only the most interesting images are shown out of the large data sets.
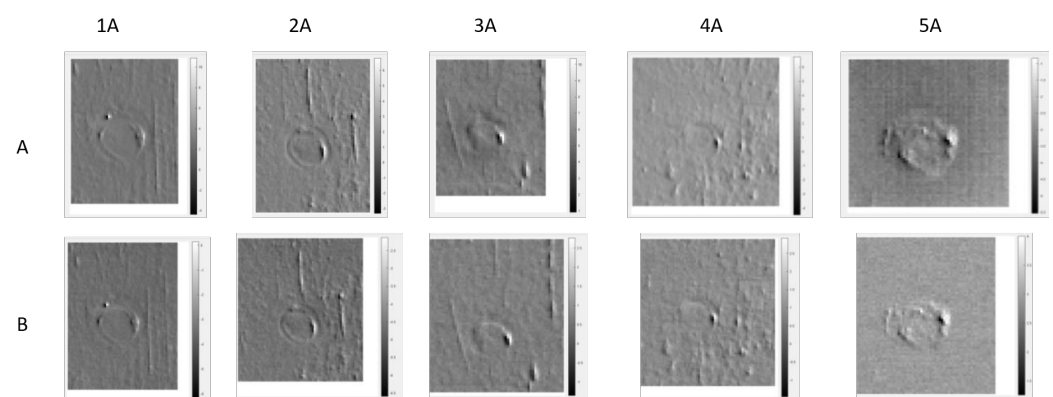
Figure 5. Images taken from the principle component analysis of the five samples during two experiments. The excitation frequency of experiment (**A**) is 0.05 Hz, and the frequency of (**B**) is 0.4 Hz.

3.2. Pulse Thermography Using Light Heating

The second light heating technique investigated in this manuscript is pulse heating. The measurement setup is visualized in Figure 2 and the parameters corresponding to 'L1', 'L2' and 'L3' can be found in Table 2. In order to investigate the influence of the pulse duration, each sample is subjected to experiments using different parameter sets. The amplitude is constant with a value of eight, which is similar to the measurements

using lock-in thermography. The parameter sets used during the pulse thermography measurements can be found in Table 6.

Table 6. Parameter combinations used during the pulse thermography measurements. The value of the amplitude is kept constant at 8 in order to ensure an adequate heating intensity.

	Parameter Set 1	Parameter Set 2
Amplitude	80%	80%
Pulse duration [s]	1	3

Figure 6 visualizes the results of the FFT analyses of the pulse thermography inspections. Similar results can be observed between experiments using pulse durations of 1 and 3 s for samples 1A, 2A and 3A; however, a longer pulse time leads to better results regarding samples 4A and 5A. Both samples 1A and 2A show a clear visible circle around the spot weld, and a different thermal behaviour between the region inside and outside the weld can be distinguished. The black regions inside the spot weld of sample 1A show a distinct phase shift, while in sample 2A, this phase shift is not visible. Sample 3A has a visible circular shape as well, but there is no phase difference between the region inside the weld and the region around it. This might mean that the weld is not optimal since no change in metallic internal structure has occurred. Similar to the lock-in measurements, sample 4A does not show a contour of the spot weld. In the images of sample 5A, a difference can be seen between the inside and outside of the spot weld, but there is no clear boundary visible. Besides the FFT analyses, principle component analyses were performed on the pulse thermography data. The results of this processing can be seen in Figure 7.
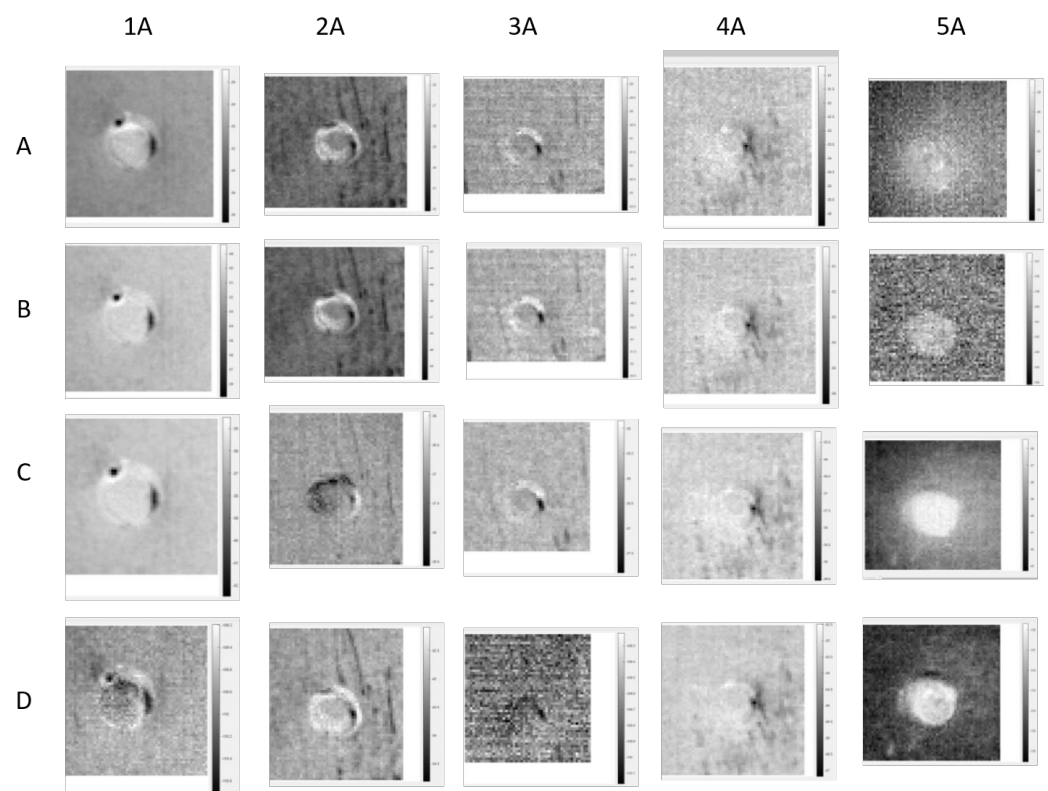
Figure 6. Snapshots taken from the fast Fourier transform analysis performed on pulse thermography data. Experiment (**A**) is performed using a pulse duration of 1s and a Fourier frequency of 0.038 Hz. Experiment (**B**) has a pulse duration of 1 s as well and is analysed using a Fourier frequency of 0.076 Hz. A pulse duration of 3 s is used for experiments (**C,D**), and the used Fourier frequencies are 0.035 Hz and 0.142 Hz.
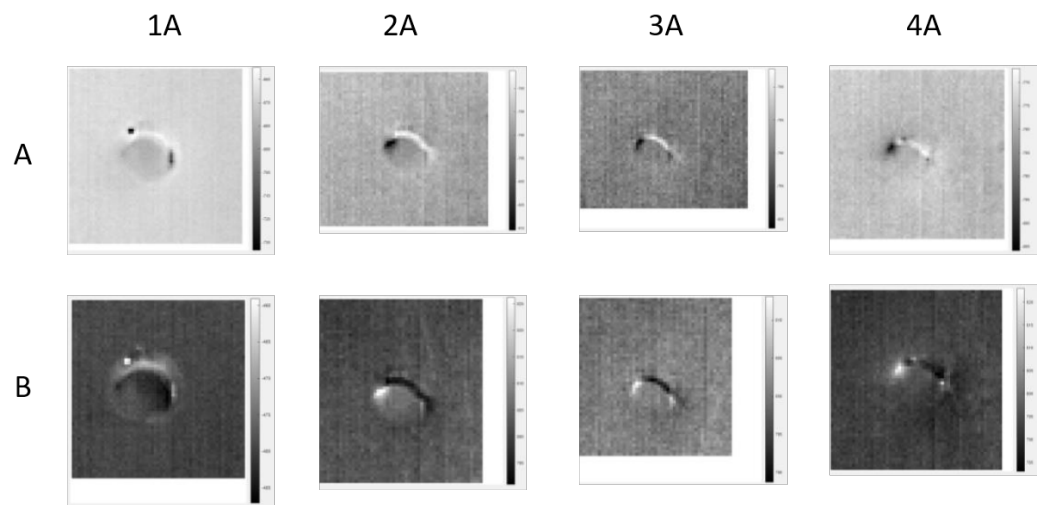
Figure 7. Results of the PCA processing of the pulse thermography data. Experiment (**A**) is conducted using an amplitude of 8 and a pulse duration of 1 s. Experiment (**B**) is conducted using the same amplitude and a pulse duration of 3 s. There are no data for sample 5A since the processing did not result in useful information. Sample shows a similar result to previous results, namely, no closed boundary can be detected.

3.3. Inductive Thermography

The five samples of the A-series are subjected to induction thermography measurements. The inspections are performed both in front and back heating, and for each heating method, three heating times are compared. The heating times can be found in Table 3.

The thermal data captured during the experiments of sample series A, using induction heating are only processed using PCA since the FFT processing did not lead to useful images. Snapshots taken from the PCA on the data captured during front heating induction are shown in Figure 8.

Besides front heating, the back of each sample is heated during three experiments. The induction times for each experiment are noted in Table 3. The thermal data are only processed using PCA since FFT did not result in useful images and can be seen in Figure 9.

Since induction thermography is a fast technique and it results in qualitative images, only this technique is used for the inspection of the remaining four B samples. The optimal parameters found during the experiments of series A can be found in Table 7. These parameters are used in the inspection of the samples of the B series.In contrast to the processing of the A series, the thermal data of the B series are processed using FFT and PCA. Both techniques resulted in decent quality images for this series. The results of the FFT processing of the front heating of the samples can be seen in Figure 10, and the PCA results can be found in Figure 11. The processed images related to back heating the sample can be seen in Figures 12 and 13.
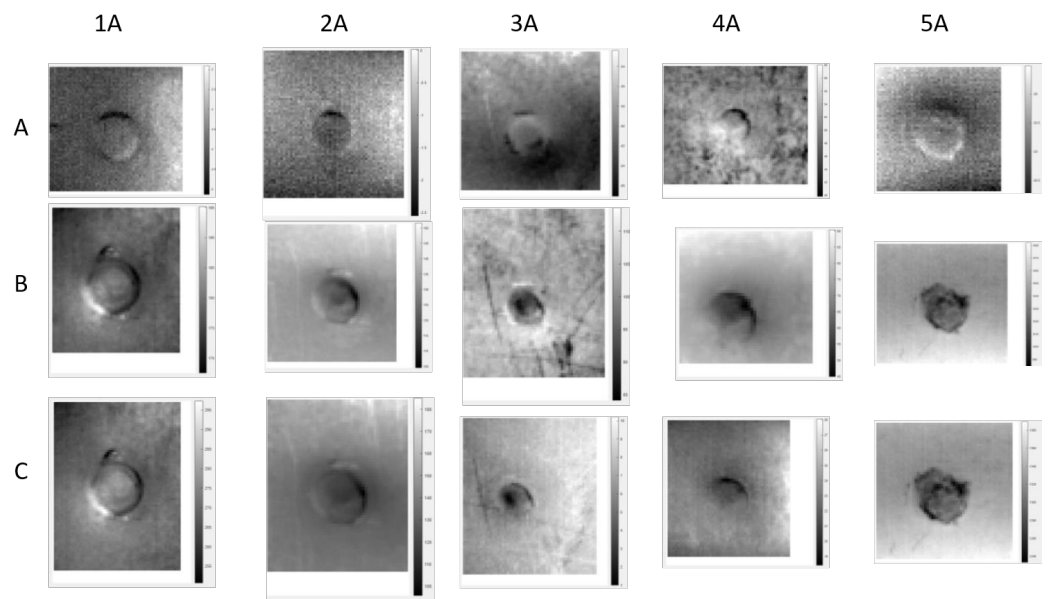
Figure 8. Images taken from the principle component analysis performed on the thermal data captured using induction heating of the front side of the sample. Experiment (**A**) is performed using an induction time of 5 s, experiment (**B**) has an induction time of 10 s, and the sample was heated for 19 s in experiment (**C**).
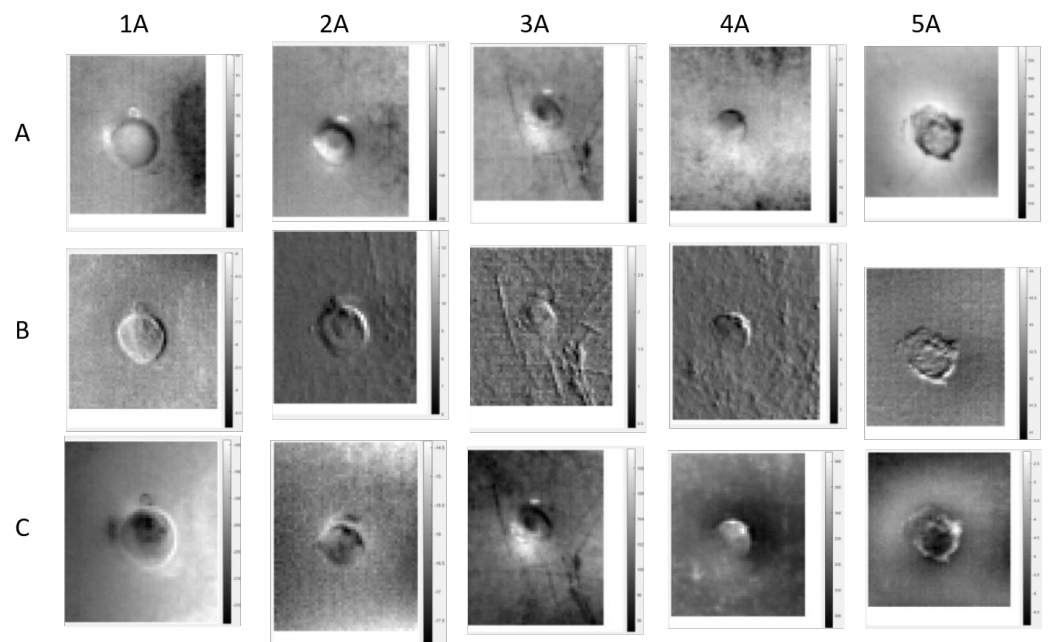
Figure 9. Processed data images from experiments performed using back heating. During experiment (**A**) an induction time of 4 s is used, during experiment (**B**) this is 8 s, and experiment (**C**) is performed using 15 s of heating.

Table 7. Best parameters found during the measurements on the A-series samples. The samples of the B series are inspected using these parameters.

	Front Induction Heating	Back Induction Heating
Excitation time [s]	19	15
Distance coil—sample [m]	0.03	0.04

1B 2B 3B 4B

A

B
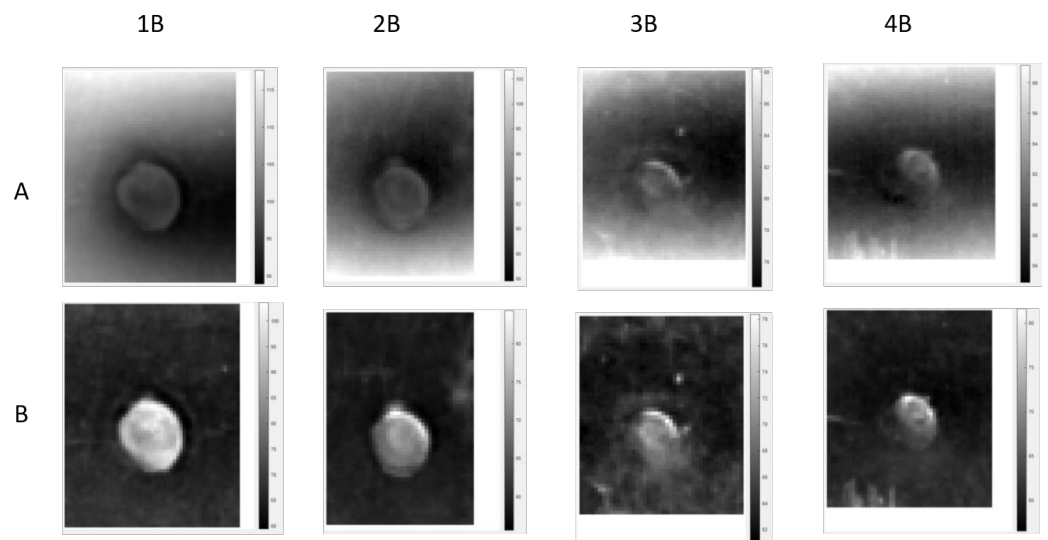
Figure 10. Results from the FFT processing of the thermal data captured using induction heating from the front side of the B-series samples. Row (**A**) shows the phase images of the measurements using an excitation duration of 19 s, and row (**B**) visualizes the amplitude images.

1B 2B 3B 4B
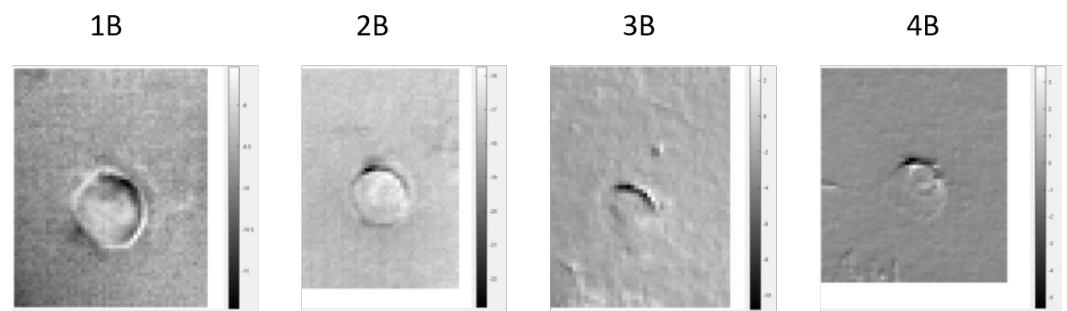
Figure 11. Snapshots taken from the principle component analysis of the thermal data of front induction heating.

1B 2B 3B 4B

A

B
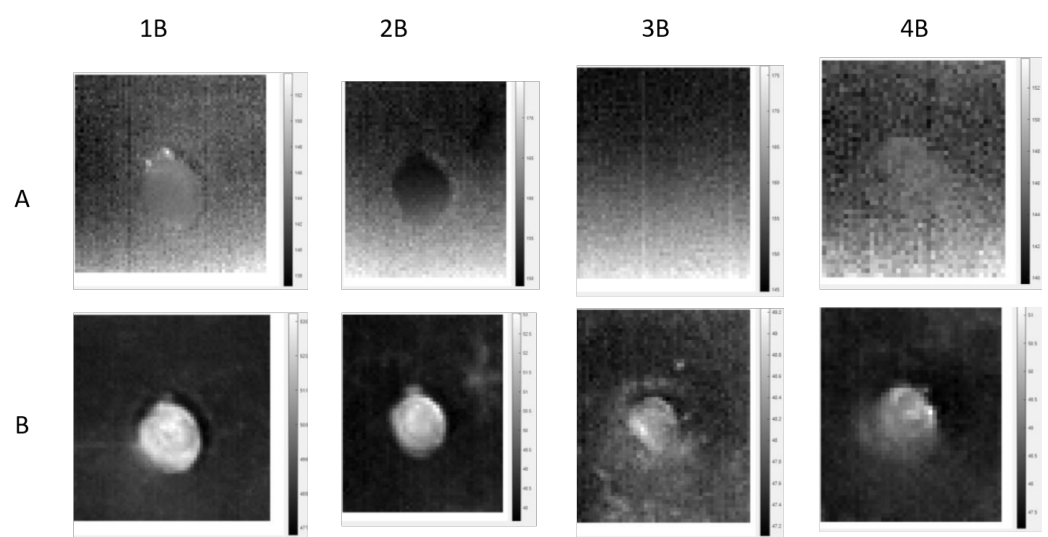
Figure 12. FFT results of the B series samples heated from the back during 15 s. Row (**A**) shows the phase images and row (**B**) the amplitude images. The phase images are not sufficient enough to make a conclusion about the spot welds, but the amplitude images show a clear difference between the regions inside and outside the spot weld.
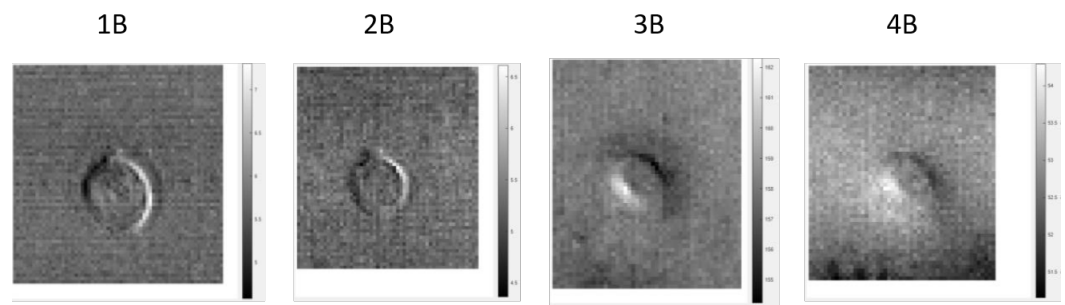
Figure 13. Results of the principle component analysis of the B-series samples heated from the back.

4. Discussion

In this manuscript, a comparison is performed between different active thermography techniques in order to find the most suitable solution for the inspection of spot welds. The samples are heated using light heating and induction heating and processed applying both fast Fourier transform and principle component analysis. As light heating excitation, both lock-in thermography and pulse thermography are investigated. For each excitation method, multiple parameter sets are explored, such as frequency variations for lock-in thermography and variations in pulse duration for pulse thermography. Induction heating shows to be the most suitable technique for spot weld inspections since it results in clear data images and low inspection times. Improving the measurements using induction thermography can be possible by minimizing the distance between the coil and the sample and increasing the amount of windings of the excitation coil. Both front and back heating result in good quality images in inductive thermography, making it possible to be used in the manufacturing process. In decent spot welds, a clear contour can be detected, and the region inside the circular boundary has a different thermal behavior in comparison to the material around the spot weld. Considering the samples used in this research, we conclude that samples 1A, 2A, 1B and 2B are the only valid spot welds.

5. Conclusions

The aim of this research was to determine the best method to perform infrared thermography during car manufacturing. Several heating techniques are not suitable to use in a manufacturing process without extensive changes, such as safety precautions. Since a car body is a complex shape, it is not always possible to inspect the welds using back heating; therefore, a solution had to be found using only front heating. An additional requirement was found in the use of robotic inspection. In order to minimize the necessity of a human inspector, it should be possible to perform the inspections automatically using a robot. Keeping these requirements in mind, the best inspection method can be found in inductive thermography. These measurements can be performed using only front heating, and the camera and heating device can be mounted on the same robot. Using induction thermography for the inspection of spot welds, it is possible to determine whether the different characteristics that determine a good weld are present or not. A proper spot weld should show a distinguishable circular shape with a closed boundary and a different thermal behaviour inside and outside the welded regions. Boundaries that are not fully closed or have an irregular shape indicate that parts of the weld are not fully melted together or the weld puddle has blown out. It is not sufficient to evaluate a spot weld only on the shape of the weld itself. In order to deliver the needed strength, the welded materials have to melt into each other inside the welding region. Therefore, it is necessary to determine whether the internal structure of the weld has changed in comparison to the surrounding area. Further investigations can be made to the induction heating in order to minimize the needed heating time. Improvements could be found in optimizing the distance between the induction spools and the sample and by increasing the amount of loops in the induction coil. In future work, the use of artificial intelligence will also be investigated in order to automatically classify spot welds.

References

1. Amosov, O.S.; Amosova, S.G.; Iochkov, I.O. Defects Detection and Recognition in Aviation Riveted Joints by Using Ultrasonic Echo Signals of Non-Destructive Testing. *IFAC-PapersOnLine* **2021**, *54*, 484–489. [CrossRef]

2. Deepak, J.R.; Bupesh Raja, V.K.; Srikanth, D.; Surendran, H.; Nickolas, M.M. Non-destructive testing (NDT) techniques for low carbon steel welded joints: A review and experimental study. *Mater. Today Proc.* **2021**, *44*, 3732–3737. [CrossRef]

3. Jasiūnienė, E.; Mažeika, L.; Samaitis, V.; Cicėnas, V.; Mattsson, D. Ultrasonic non-destructive testing of complex titanium/carbon fibre composite joints. *Ultrasonics* **2019**, *95*, 13–21. [CrossRef] [PubMed]

4. Rivas, S.; Servent, R.; Belda, J. Automated Spot Weld Inspection In The Automotive Industry. *e-J. Nondestruct. Test.* **2005**, *10*, 36–43.

5. Runnelmalm, A.; Appelgren, A. SpotLight Punktsvetsning för Lättviktskonstruktioner Resistance Spot Welding for Light Weight Design WP 5 Automated Quality Checking of Spot Welds Evaluation of Non-Destructive Testing Methods for Automatic Quality Checking of Spot Welds. Available online: http://hv.diva-portal.org/smash/get/diva2:642618/FULLTEXT01.pdf (accessed on 11 March 2022).

6. Athi, N.; Wylie, S.R.; Cullen, J.D.; Al-Shamma', A.I.; Sun, T. Ultrasonic Non-Destructive Evaluation for Spot Welding in the Automotive Industry. In Proceedings of the SENSORS, Christchurch, New Zealand, 25–28 October 2009. [CrossRef]

7. Santos, T.G.; VilaCca, P.; Quintino, L.; Dos Santos, J.; Miranda, R.M. Application Of Eddy Current Techniques To Inspect Friction Spot Welds In Aluminium Alloy Aa2024 and a Composite Material. *Weld. World* **2011**, *55*, 12–18. [CrossRef]

8. Sherepenko, O.; Mohamadizadeh, A.; Zvorykina, A.; Worswick, M.; Biro, E.; Jüttner, S. Determination of resistance spot weld failure path in ultra-high-strength press-hardened steel by control of fusion boundary transient softening. *J. Mater. Sci.* **2021**, *56*, 14287–14297. [CrossRef]

9. Yang, Z.W.; Yan, H.P.; Li, Y.; Kou, G.J.; Tian, G.; Zhang, W. A Novel Inclined Excitation Method for Crack Detection of Non-Ferromagnetic Materials Using Eddy Current Thermography. *Strength Mater.* **2019**, *51*, 558–568. [CrossRef]

10. Oswald-Tranta, B. Lock-in inductive thermography for surface crack detection in different metals. *Quant. Infrared Thermogr. J.* **2019**, *16*, 276–300. [CrossRef]

11. Runnemalm, A.; Ahlberg, J.; Appelgren, A.; Sjökvist, S.; Runnemalm, A.; Ahlberg, J.; Appelgren, A.; Sjökvist, S. Automatic Inspection of Spot Welds by Thermography. *J. Nondestruct. Eval.* **2014**, *33*, 398–406. [CrossRef]

12. Kastner, L.; Ahmadi, S.; Jonietz, F.; Jung, P.; Caire, G.; Ziegler, M.; Lambrecht, J. Classification of Spot-Welded Joints in Laser Thermography Data Using Convolutional Neural Networks. *IEEE Access* **2021**, *9*, 48303–48312. [CrossRef]

13. Schlichting, J.; Brauser, S.; Pepke, L.A.; Maierhofer, C.; Rethmeier, M.; Kreutzbruck, M. Thermographic testing of spot welds. *NDT E Int.* **2012**, *48*, 23–29. [CrossRef]

14. Jonietz, F.; Myrach, P.; Suwala, H.; Ziegler, M. Examination of Spot Welded Joints with Active Thermography. *J. Nondestruct. Eval.* **2016**, *35*, 1–14. [CrossRef]

15. Usamentiaga, R.; Ibarra-Castanedo, C.; Klein, M.; Maldague, X.; Peeters, J.; Sanchez-Beato, A. Nondestructive Evaluation of Carbon Fiber Bicycle Frames Using Infrared Thermography. *Sensors* **2017**, *17*, 2679. [CrossRef] [PubMed]

16. Maldague, X.; Galmiche, F.; Ziadi, A. Advances in pulsed phase thermography. *Infrared Phys. Technol.* **2002**, *43*, 175–181. [CrossRef]